Evaluation of predicted knee function for component malrotation in total knee arthroplasty

Vanheule, Valentine; Delport, Hendrik Pieter; Andersen, Michael Skipper; Scheys, Lennart; Wirix-Speetjens, Roel; Jonkers, Ilse; Victor, Jan; Vander Sloten, Jos

Published in:
Medical Engineering & Physics

DOI (link to publication from Publisher):
10.1016/j.medengphy.2016.12.001

Publication date:
2017

Document Version
Accepted author manuscript, peer reviewed version

1. Title page

Evaluation of predicted knee function for component malrotation in total knee arthroplasty

Valentine Vanheule[a,b], Hendrik Pieter Delport[c], Michael Skipper Andersen[d], Lennart Scheys[c], Roel Wirix-Speetjens[b], Ilse Jonkers[e], Jan Victor[f] and Jos Vander Sloten[a]

[a]Biomechanics section, Katholieke Universiteit Leuven, Celestijnenlaan 300C, 3001 Leuven, Belgium
[b]Materialise N.V., Technologielaan 15, 3001 Leuven, Belgium
[c]Department of Orthopaedics, University Hospital Pellenberg, Katholieke Universiteit Leuven, Weligerveld 1, 3212 Pellenberg, Belgium
[d]Department of Mechanical and Manufacturing Engineering, Aalborg University, Fredrik Bajers Vej 5, 9100 Aalborg, Denmark
[e]Department of Kinesiology, Katholieke Universiteit Leuven, Tervuursevest 101, 3001 Leuven, Belgium
[r]Department of Physical Medicine and Orthopedic Surgery, Ghent University, De Pintelaan 185, 9000 Ghent, Belgium

Corresponding author

Valentine Vanheule

Department of Mechanical Engineering
Division BMe
Celestijnenlaan 300C
3001 Leuven, Belgium
valentine.vanheule@kuleuven.be

Phone: +32 16 74 42 71
Fax: +32 16 39 66 00

2. Abstract

Soft-tissue balancing for total knee arthroplasty (TKA) remains subjective and highly dependent on surgical expertise. Pre-operative planning may support the clinician in taking decisions by integrating subject-specific computer models that predict functional outcome. However, validation of these models is essential before they can be applied in clinical practice. The aim of this study was to evaluate a knee modelling workflow by comparing experimental cadaveric measures to model-based kinematics and ligament length changes. Subject-specific models for three cadaveric knees were constructed from medical images. The implanted knees were mounted onto a mechanical rig to perform squatting, measuring kinematics and ligament length changes with optical markers and extensometers. Coronal malrotation was introduced using tibial inserts with a built-in slope. The model output agreed well with the experiment in all alignment conditions. Kinematic behaviour showed an average RMSE of less than 2.7 mm and 2.3° for translations and rotations. The average RMSE was below 2.5% for all ligaments. These results show that the presented model can quantitatively predict subject-specific knee behaviour following TKA, allowing evaluation of implant alignment in terms of kinematics and ligament length changes. In future work, the model will be used to evaluate subject-specific implant position based on ligament behaviour.

Keywords: subject-specific, alignment, soft tissue balancing, kinematic knee rig, in vitro

3. Introduction

Creating appropriate soft-tissue balance during total knee replacement surgery is mainly subjective and highly dependent on the surgeon's expertise [1,2]. Pre-operative planning incorporating predictive tools to evaluate functional outcome may support the surgeon by comparing different surgical treatments. Subject-specific musculoskeletal models have a high potential to be used as a predictive tool in clinical practice [3]. In detailed joint models, ligaments strongly influence kinematics since they are highly important structures for guiding and stabilising knee motion [4,5]. However, before applying such models in a clinical setting, validation is of paramount importance. The purpose of this study was to evaluate a computational efficient model that can predict subject-specific knee kinematics and ligament length changes for different implant alignments.

Recently, several studies explored methods that can simultaneously compute motions as well as muscle and contact forces. Hast and Piazza presented a dual-joint workflow in which the knee joint is alternated between a simplified knee joint representation for inverse dynamics and an unconstrained knee with elastic foundation contact [6]. Thelen et al. extended the computed muscle control algorithm (CMC) to co-simulate muscle and contact forces, using an elastic foundation model [7]. Guess et al. presented a two-stage modelling method, an inverse kinematics and a forward dynamics simulation, predicting muscle and contact forces concurrently [8].

Andersen et al. introduced an alternative approach, called force-dependent kinematics (FDK), that extends the fast inverse dynamic simulations with the ability to estimate secondary joint kinematics [9]. This method relies on an assumption of quasi-static force equilibrium in the secondary joint kinematics at each time step during the analysis. In 2014, the FDK method was applied and knee contact forces were validated during walking activities in the winning model of the Grand Challenge competition [10].

Musculoskeletal models have the ability to explore the relationship between implant alignment and functional outcome for different activities of daily living. Others investigated the effects of implant alignment variation during a simulated squat, however, without collecting experimental evidence for the malaligned configurations [11,12]. In our study, we modelled different implant alignment variations and additionally, performed a cadaveric study to validate the predicted knee function for each alignment. FDK was used to simulate knee kinematics and predict ligament length change patterns for three cadaveric knees with TKA performing a squat motion. In addition to the standard implant, malrotation in the coronal plane was introduced by using tibial inserts with a built-in varus or valgus offset [13]. For each specimen, three squats were performed with the knee in neutral, varus or valgus alignment. The model outputs were validated by comparing experimental and model-predicted tibio-femoral motion and ligament length changes. To our knowledge, this is the first study to both simulate and validate the impact of implant alignment on kinematics and ligament length changes as predicted by computer models.

4. Methods

4.1. Experimental data collection

4.1.1. Specimen preparation and imaging

Three cadaveric knee specimens were used for squat simulations in a dynamic knee simulator system. The methodology of the specimen preparation was similar to the workflow described by Victor et al. [14]. The study protocol was approved by the local Ethics Committee.

After thawing the fresh frozen specimens, full leg T1-weighted opposed-phase spoiled gradient echo magnetic resonance imaging (MRI) scans were obtained using a 3T scanner (Ingenia, Philips Healthcare) to visualise soft tissues. The slice thickness was 2 mm and all slices had an in plane resulotion of 0.9 mm x 0.9 mm. Subsequently, frames (Medtronic, MN, USA) with

reflective spherical markers were rigidly attached to femur, tibia and patella. Each frame carried 4 markers, which were 6 mm in diameter. The femoral frame was inserted within 21 cm from the joint line, the tibial frame within 18 cm from the joint line and the patellar frame was inserted onto the patella. To allow accurate three-dimensional motion tracking, a six-camera motion capture system (Vicon MX40, Oxford, UK) was used. The optical markers could accurately be located on the pre-operative and post-operative computed tomography (CT) scans.

Volumetric CT scans of the full lower leg with the attached markers were obtained on a dual-source multidetector CT scanner (SOMATOM Definition Flash, Siemens), equipped with two 64-detector row units, using a slice thickness of 0.75 mm and a pitch of 0.8 mm/rev. The images were processed in Mimics v. 17.0 (Materialise, Leuven, Belgium) to construct the bone models of femur, tibia and patella. These bone geometries were used to identify bony landmarks.

Next, the hip and foot were removed from the full leg, with a femoral cut 32 cm proximal of the joint line and a tibial cut 28 cm distal from the joint line. The quadriceps muscle was dissected and its preserved tendon was fixed into a clamp. In addition, the semitendinosus together with the semimembranosus muscle, as well as the biceps femoris muscle were dissected and suture wires were attached to the preserved tendons. The proximal femur and distal tibia were then embedded in aluminium containers, preserving the physiologic alignment in the coronal plane and parallel with the container in the sagittal plane.

Two extensometers (MTS, Eden Prairie, MN, USA) were sutured to the medial and lateral collateral ligaments by an experienced surgeon. The fixation of the extensometers was centred over the joint line, on an unloaded and fully extented knee [15]. During the measurements, ligament length change relative to the extended knee was calculated using the formula $\varepsilon = (L - L_r)/L_r$, where L was the instantaneous length of the extensometer arms connected to the ligament and L_r was the reference length at full extension.

4.1.2. Total knee replacement and imaging

An experienced surgeon (HD) performed the total knee arthroplasty on each specimen using a posterior-stabilised total knee arthroplasty (Performance, Biomet Inc., Warsaw, IN, USA). In addition to the tibial implant placed with standard alignment instrumentation, two variations of the tibial insert were designed through additive manufacturing. These variations were able to artificially simulate a TKA coronal malalignment by their built-in varus or valgus design. The inserts were modelled so that the central height was preserved while making one side thicker and the other side thinner than the neutral insert. For each specimen, three squat trials were performed. Specimen 1 underwent squats with neutral insert, 5° varus insert and 5° valgus insert. Specimen 2 and 3 underwent squats with neutral insert, 3° varus insert and 3° valgus insert. The tibial insert thickness for specimen 2 and 3 was smaller, leading to a smaller varus and valgus angle due to design limitations. The valgus insert squat of specimen 3 is not shown in the results since the quadriceps ruptured during the last experiment.

After the trials, post-operative CT scans were made with the optical markers still attached on the same scanner as the pre-operative scans, allowing to accurately document the implant position.

4.1.3. Knee simulator set-up

The specimens were mounted onto a dynamic knee simulator system, based on the Oxford rig [16]. This mechanical system permits six degrees-of-freedom (DOFs) for both the tibio-femoral and the patello-femoral joint. The femoral container was connected to an artificial hip assembly and the tibial container to an artificial ankle assembly. The quadriceps clamp was connected to an actuator that could apply a variable quadriceps load. Both hamstring wires were connected with constant-force springs of each 50 N (Type KKF 8077, Lesjöfors, Karlstad, Sweden). The hip assembly could slide vertically and flex and extend, the ankle assembly allowed rotation in

all three directions and translated medio-laterally. Sensors detected the quadriceps force, ankle force and relative hip height and these real-time data were processed in a closed feedback system (LabVIEW, National Instruments, Texas, USA), allowing the performance of a squat motion by moving the hip assembly and applying a variable quadriceps force to induce a vertical ankle force of 111 N. The quadriceps load increased during knee flexion, starting from a few hundred Newton at the beginning of the experiment and the load could go up to 2000 N at deep knee bend. A full squat motion began around 30-40° knee flexion and went up to 110-120°. The squat did not begin at full extension to prevent hyperextension [14].

Six infrared emitting cameras (MX40, Vicon, Oxford, UK) tracked the reflecting light from the rigidly attached optical markers on femur, tibia and patella at a sampling frequency of 100 Hz. This provided us an accurate measurement of the knee joint motion during squat. Throughout knee flexion, the three-dimensional (3D) coordinates of the passive markers were tracked and the relative position of all the important landmarks on femur and tibia were computed. The distance between the ligament insertion points on femur and tibia or fibula was used as the ligament length at any given position in the flexion arc of the knee joint.

4.2. Computational model definition

4.2.1. Subject-specific knee model set-up

The experimental set-up was implemented into the AnyBody Modeling System 6.0.5 (AnyBody Technology A/S, Denmark). The knee model consisted of the subject-specific bone geometry segmented from CT scans in Mimics 17.0 (Materialise N.V., Leuven, Belgium). The implant position was determined by the post-operative CT scans. The contact between femoral and tibial implant and between femoral implant and patella was modelled using a rigid-rigid STL-based contact model. The contact forces were computed based on the penetration depth, d_i, of a vertex

into the opponent surface. The penetration volume V_i was approximated by the multiplication of the penetration depth and the opponent triangle area A_i, so that for the ith vertex

$$V_i = A_i d_i \qquad (1)$$

The direction of the contact force was determined by the normal of the triangle and the contact force magnitude for each contributing element was computed using a linear force law between the penetration volume and the pressure module P

$$F_i = PV_i \qquad (2)$$

A pressure module of 4.6 GN/m^3 was used, based on previous tests where the trade-off between the penetration depth and the numerical issues of solving contact between two surfaces with high stiffness was investigated [10].

Four ligaments were defined: proximal and distal part of the medial collateral ligament (MCL), lateral collateral ligament (LCL), medial patello-femoral ligament (MPFL) and lateral epicondylo-patellar ligament (LEPL). The insertions were estimated based on an anatomical atlas using the specimen's bony landmarks and two insertion sites of the MCL proximally and distally on the tibia were identified (MCLprox and MCLdist) [14]. Ligaments were represented as non-linear line segments that wrap over analytical surfaces approximating the relevant geometries. One cylinder was placed medially on the tibia to allow the MCLdist to wrap around the medial tibial condyle and another cylinder was fitted to the femoral implant to prevent the quadriceps muscle from penetrating the implant during deep flexion. Two ellipsoids were introduced to wrap the MPFL and LEPL around the femoral condyles (Figure 1).

Ligament force was modelled with the following force-displacement relationship [17]

$$f = \begin{cases} 1/4k\varepsilon^2/\varepsilon_l & 0 \le \varepsilon \le 2\varepsilon_l \\ k(\varepsilon - \varepsilon_l) & \varepsilon > 2\varepsilon_l \\ 0 & \varepsilon < 0 \end{cases}, \qquad (3)$$

where f is the tensile force, k the ligament stiffness, ε_l the linear strain limit set at 0.03 [18] and ε the strain calculated with the ligament length L and its zero-load length L_0 using the equation $\varepsilon = (L - L_0)/L_0$. The zero-load length L_0 was computed using the following definition:

$$L_0 = L_r/(\epsilon_r + 1) \qquad (4)$$

in which L_r is the ligament reference length and ϵ_r the reference strain. The stiffness and reference strain of MCL and LCL were based upon values given by Blankevoort and Huiskes and can be found in Table 1 [17]. The ligament reference lengths were computed with the intact knee in full extension. Not much information is available regarding the stiffness and reference strain of the patellar ligaments MPFL and LEPL. The MPFL is the primary restraint to lateral patellar displacement and lateral soft-tissues contribute less to the overall stability [19]. Accordingly, MPFL stiffness was chosen in the same range of MCL and LCL and lower values were attributed to LEPL. Since patellar ligaments are tightest in full extension and slacken with flexion, positive reference strain values were assigned in the same range of MCL and LCL [19]. Both MPFL and LEPL were represented by three line segments and their parameter values are shown in Table 1.

To compare the model output to the local extensometer length changes, the reported model ligament length changes were calculated using the formula $\varepsilon_{model} = (L - L_r)/L_r$. Additional to the extensometer length changes, kinematic based ligament length changes were measured by tracking the length changes of the ligament line segment during the experimental motion compared to the length at full extension.

The simulation mimicked the experimental set-up, such that the same force to the quadriceps tendon was applied and the same vertical motion of the hip assembly was generated. Figure 2 shows how the model was constrained during the simulation. The hip assembly could move up

and down and flex and extend. The ankle assembly could rotate in all three directions and could move medio-laterally. Consequently, this configuration provided the tibio-femoral joint with all six DOFs. The patello-femoral joint was modelled with the assumption of a constant length of the patellar tendon, while the three translational DOFs and the spin and tilt (patellar rotation around respectively the anterior-posterior axis and the proximal-distal axis) were solved by the FDK solver. A simple linear torsional spring with spring constant of 100 Nm/rad was included to ensure some stiffness in the patellar tilt direction during deep knee flexion when the patellar ligaments were slack.

4.2.2. Force-dependent kinematics

Knee kinematics were simulated using FDK, an extended inverse dynamics approach, which simultaneously computes ligament forces and secondary joint motions [10]. This methodology relies on an assumption of quasi-static force equilibrium in the secondary joint kinematics at each time step during the analysis, eliminating the need for time integration. This assumption of static equilibrium only applies to the FDK directions and the full dynamics in all other DOFs are taken into account. This modelling approach is implemented into the AnyBody Modeling System (AnyBody Technology, A/S, Aalborg, Denmark).

4.3. Data analysis

4.3.1. Sensitivity study

A sensitivity analysis was performed to investigate the influence of the tibio-femoral model parameters on the output. The insertion points of three ligament line segments (MCLprox, MCLdist and LCL) as well as the patellar tendon were moved from their reference position. Since the attachment of these structures is known to lay on the bone surface, the attachments were varied in a plane tangent to the bone surface.

From a study investigating the precision in locating landmarks on CT scans, an estimate of the appropriate variability was made [14]. In the study, an intra-variability of around 1 mm and the inter-variability was 3.5 mm or less was reported. Based on these results, a variation of 3.5 mm was first chosen, representing a range of 7 mm.

Consequently, all ligaments insertions were varied from -3.5 mm to +3.5 mm in the anterior-posterior and proximal-distal direction. The insertions of the patellar tendon were varied from -3.5 mm to +3.5 mm in the medial-lateral and anterior-posterior direction. When one of the insertion locations was changed, the reference ligament length was recalculated and updated prior to the simulation.

In addition, the stiffness and reference strain of the three ligament line segments were varied, each from +3.5% to -3.5% of their reference value. A total of 45 configurations were analysed and the overview of these simulations can be found in Table 2.

4.3.1. Metrics

The tibio-femoral rotations were derived using the Grood and Suntay protocol and the translations were reported in the tibial reference frame [20]. Positive values were assigned to medial, anterior and proximal translations and to valgus and external tibial rotations. Each of these trials show the downwards motion of a squat.

The differences between the experimental and simulation results were quantified using the Root-Mean-Square-Error (RMSE) and the Pearson correlation coefficient with ρ categorized as $\rho \leq 0.35$, $0.35 < \rho \leq 0.67$, $0.67 < \rho \leq 0.9$, $0.9 < \rho$ to be weak, moderate, strong or excellent correlations[21,22]

5. Results

The computed tibio-femoral translations (Figure 3) and rotations (Figure 4) showed a good agreement, predicting the proximal-distal, medial-lateral, anterior-posterior, varus-valgus, internal-external motions with an average RMSE of respectively 1.0 mm, 1.2 mm, 2.7 mm, 0.7° and 2.3°. The average Pearson correlation coefficient for the aforementioned motions was 1.00, 0.38, 0.85, 0.93 and 0.95, showing strong or excellent correlations except for the medial-lateral motion. This lower correlation is caused by the low order of magnitude of this motion. An overview of the kinematic RMSE and Pearson correlation coefficient for all trials for each cadaver can be found in Table 3.

Additionally, tibio-femoral motion can be more intuitively analysed when the 3D motion is projected onto a two-dimensional (2D) plane. Figure 5 shows the projected tibio-femoral kinematics during squat. Because of the clinical importance of rotational movement, the projection plane of choice was the tibial horizontal plane. This plane is defined as the plane perpendicular to the tibial mechanical axis and comprises the line connecting the tibial condyle centres. The projections of the centres of the medial and lateral femoral condyles onto the tibial horizontal plane were presented for different flexion angles, namely 40°, 60°, 80° and 100°.

An overview of the ligament length change RMSE and Pearson correlation coefficient for all trials for each specimen can be found in Table 4. The lateral extensometer length change was compared to the model LCL length change and the medial extensometer length change was compared to the model MCLdist length change. The average RMSE was 2.7% for MCLdist and 4.0% for LCL and the average Pearson correlation coefficient was 0.96 and 0.74 for MCLdist and LCL respectively. Figure 6 depicts the predicted subject-specific model length changes compared to the kinematic based experimental length changes for all conditions. The average RMSE was 0.9% for MCLdist and 2.5% for LCL and the average Pearson correlation coefficient was 0.99 and 0.98 for MCLdist and LCL respectively.

Figure 7 shows the results of the sensitivity study for the three specimens for the neutral insert trial. The translations were the least sensitive to changes in model parameters. The largest changes can be found in internal-external rotation and ligament length changes, presenting changes up to 3.8° in the maximum internal tibial rotation at the end of the simulation, and up to 6.4% in the absolute ligament length change at the end of the simulation. The perturbed simulations of specimen 2 failed to solve if MCL was less strained, hence we removed these failed output resulting in a smaller shaded area for MCL.

6. Discussion

The motivation of this work was to develop a computational efficient subject-specific model that can predict the relative impact of different implant configurations on kinematics and ligament length change patterns. A validation was performed using *in vitro* kinematics and ligament length changes of different component alignments for three different subjects.

The results showed that the kinematics can accurately be predicted, showing an average RMSE of less than 2.7 mm and 2.3° for translations and rotations. The largest RMSE was for anterior-posterior translation. The model consistently underestimated the anterior position of the femur with respect to the tibia during the beginning of the squat, indicating that some anterior-posterior stiffness is missing. In reality, the knee joint is surrounded by the joint capsule membrane, which is lacking in the model. Overall, the kinematics showed an excellent correlation and small RMSE for the three subjects during the three different alignment conditions. The motions are comparable in trend and in magnitude with the results of Baldwin et al., who validated a finite element (FE) knee model with a posterior-stabilised implant for three cadaveric knees inside a mechanical rig [23]. The ligament parameters and attachment sites were optimised by minimising differences between model-predicted and experimental kinematics. They noted average RMSE of less than 1.8 mm and 2.2° for translations and rotations respectively. Without ligament parameter optimisation, our model achieved similar

results. Moreover, the predicted kinematics after component malrotation showed comparable RMSE.

To evaluate the differences caused by malalignment, the different rows for one specimen can be compared in Figure 5. Valgus malalignment resulted in a more externally rotated starting position of the tibia, whereas varus malalignment caused a slightly more internally rotated tibia compared to the neutral alignment. This presents a direct link to ligament behaviour, since the collateral ligaments are known to be important stabilisers. MCL was more strained in valgus and acts as a restraint to tibial internal rotation, LCL experienced more strain in varus, increasing the restraint to tibial external rotation [24].

Next to changes introduced by coronal malalignment, the inter-specimen variability influenced the kinematics as well. Even though the contact geometry was identical for all specimens, different kinematic behaviour between the specimens can be seen, in particular with respect to the amount of anterior-posterior translation. Nevertheless, the model was able to closely match the experimental kinematics for each specimen. All specimens showed posterior femoral rollback laterally, abnormal anterior femoral translation medially was present for Specimen 1. Similar inter-specimen variability of kinematics after TKA was also seen *in vivo* [23]. Abnormal anterior motion was mostly attributed to lack of PCL and unbalanced collateral ligaments [26]. This explanation seems plausible, since anterior translation was mostly present for varus malalignent of Specimen 1, where 5° of malalignment was introduced as opposed to the 3° of malalignment in Specimen 2 and 3. During varus malrotation, MCL was more slack, resulting in more instability.

From the sensitivity study, it is clear that the ligament length change is sensitive to the model parameters. However, the trend of ligament behaviour as a function of implant alignment can be captured by the model. When comparing the extensometer length changes to the model, an excellent average correlation of 0.96 and RMSE of 2.7% was seen for MCL, while LCL had a

strong average correlation of 0.74 and an RMSE of 4.0%. Extensometer length changes are local length changes measured at the mid-region of the ligament, whereas the reported model length changes show average length changes between the insertion points. Hence, additional to the local extensometer length changes, the kinematic based ligament length changes were reported, since experimental ligament length changes are often described using the length between the ligament insertions during the reproduced motion [27]. In our study, these kinematic based length changes showed a strong to excellent correlation and the average RMSE is below 2.5% for all ligament segments. The local extensometer and kinematic based experimental length changes agreed well for MCL, while showing larger deviations for LCL, indicating that the simple ligament model cannot fully represent the variable behaviour of the LCL.

This study investigated the relative behaviour of ligament length changes when varying implant alignment. When introducing the different configurations for the tibial insert, the model and kinematic based experimental strains showed an analogous behaviour. This behaviour is consistent with the results of Delport et al. [28]. They reported that both for the neutral aligned as for the varus or valgus configurations, MCL as well as LCL remained isometric in the beginning of the squat and then started to relax. In addition, the relative relationship between the varus, neutral and valgus alignment corresponds well to our results, resulting in more MCL strain and less LCL strain for valgus malalignment and the other way around for varus malalignment.

The use of mechanical knee simulators in validation studies is a cost-effective and controlled method to mimic real-life conditions. However, this set-up differs from the actual physiologic loading condition, for instance keeping the hip fixed over the ankle and the constant hamstrings load. Despite this artificial representation, the knee motions agree well with *in vivo* motions, supporting the use of such rigs as an intermediate step towards clinical application. Two studies

of Victor et al. looked at knee motions, one in a mechanical rig [14] and one in real patients [29]. The *in vitro* study with cadaver knees in a mechanical rig showed mean ranges of motion for tibial rotation and for posterior translation of the medial and lateral femoral condyle of respectively 9.7°, 12.9 mm and 16.3 mm for a PS implant [14]. In the second study, *in vivo* kinematics were measured in TKA patients during deep knee bend with the help of dynamic fluoroscopy [29]. The average range of the aforementioned motions was 10.8°, 14 mm and 23 mm.

The results of the current study need to be seen within the light of the following limitations. The same implant type was used in all three specimens, which meant sacrificing the cruciate ligaments. Cruciate-retaining implants were not tested. Furthermore, the reported extensometer values show only the ligament length changes at the location where the extensometer is sutured. However, ligaments show different length change behaviour at different locations. Ligament model parameters were based on values from literature to demonstrate the generic workflow. However, it is known that ligament zero-load lengths are sensitive parameters in computational models but difficult to measure [30–32]. Other studies often optimize these zero-load lengths until the rotational knee behaviour matches the experimental data [33]. Finally, only coronal implant position variation is modelled here. In future work, we plan to investigate other implant configuration such as joint line variation.

In summary, this work presented a model-based and experimental evaluation of the prediction of knee kinematics and ligament length changes for three different subjects following TKA. Malalignment was introduced and the associated changes in knee kinematic and ligament length change patterns could be predicted well by the model. Despite the identical implant geometry, inter-specimen differences were both experimentally observed and predicted by the subject-specific model. This validation study is a first, necessary step towards the clinical application of musculoskeletal models. Model credibility to predict component malalignment was assured

392 in this work and the current results support the potential of subject-specific musculoskeletal
393 modelling to aid surgeons in deciding the optimal implant configuration for a patient.

394 **Conflict of interest**

395 The authors declare that they have no conflicts of interest.

396 **7. Acknowledgments**

397 This work has financial support by the Baekeland scheme of the agency for Innovation by
398 Science and Technology (IWT) under grant number IWT 110554 to V. Vanheule and the
399 Danish Council for Independent Research (DFF) under grant number DFF-4184-00018 to M.
400 S. Andersen.

401

402

403

404

405

406

407

408

409

410

411

412

8. References

[1] Griffin FM, Insall JN, Scuderi GR. Accuracy of soft tissue balancing in total knee arthroplasty. J Arthroplasty 2000;15:970–3.

[2] Abdel MP. Measured resection versus gap balancing for total knee arthroplasty. Clin Orthop Relat Res 2014;472:2016–22.

[3] Fregly BJ, Besier TF, Lloyd DG, Delp SL, Banks SA, Pandy MG, et al. Grand challenge competition to predict in vivo knee loads. J Orthop Res 2012;30:503–13.

[4] Amiri S, Cooke D, Kim IY, Wyss U. Mechanics of the passive knee joint. Part 2: interaction between the ligaments and the articular surfaces in guiding the joint motion. Proc Inst Mech Eng Part H J Eng Med 2007;221:821–32.

[5] Wilson DR, Feikes JD, O'Connor JJ. Ligaments and articular contact guide passive knee flexion. J Biomech 1998;31:1127–36.

[6] Hast MW, Piazza SJ. Dual-joint modeling for estimation of total knee replacement contact forces during locomotion. J Biomech Eng 2013;135:021013.

[7] Thelen DG, Won Choi K, Schmitz AM. Co-Simulation of Neuromuscular Dynamics and Knee Mechanics During Human Walking. J Biomech Eng 2014;136:021033.

[8] Guess TM, Stylianou AP, Kia M. Concurrent prediction of muscle and tibiofemoral contact forces during treadmill gait. J Biomech Eng 2014;136:021032.

[9] Andersen MS, Damsgaard M, Rasmussen J. Force-dependent kinematics : a new analysis method for non-conforming joints. 13th Bienn. Int. Symp. Comput. Simul. Biomech., 2011.

[10] Marra MA, Vanheule V, Rasmussen J, Verdonschot NJJ, Andersen MS. A Subject-Specific Musculoskeletal Modeling Framework to Predict in Vivo Mechanics of Total Knee Arthroplasty. J Biomech Eng 2014;137:020904.

[11] Thompson JA, Hast MW, Granger JF, Piazza SJ, Siston RA. Biomechanical effects of total knee arthroplasty component malrotation: A computational simulation. J Orthop Res 2011;29:969–75.

[12] Chen Z, Wang L, Liu Y, He J, Lian Q, Li D, et al. Effect of component mal-rotation on knee loading in total knee arthroplasty using multi-body dynamics modeling under a simulated walking gait. J Orthop Res 2015;33:1287–96.

[13] Werner FW, Ayers DC, Maletsky LP, Rullkoetter PJ. The effect of valgus/varus malalignment on load distribution in total knee replacements. J Biomech 2005;38:349–55.

[14] Victor J, Bellemans J. A comparative study on the biomechanics of the native human knee joint and total knee arthroplasty. Dep Orthop Fac Med 2009;PhD.

[15] Delport H, Labey L, De Corte R, Innocenti B, Vander Sloten J, Bellemans J. Collateral ligament strains during knee joint laxity evaluation before and after TKA. Clin Biomech 2013;28:777–82.

[16] Zavatsky AB. A kinematic-freedom analysis of a flexed-knee-stance testing rig. J Biomech 1997;30:277–80.

[17] Blankevoort L, Huiskes R. Ligament-bone interaction in a three-dimensional model of the knee. J Biomech Eng 1991;113:263–9.

[18] Butler DL, Kay MD, Stouffer DC. Comparison of material properties in fascicle-bone units from human patellar tendon and knee ligaments. J Biomech 1986;19:425–32.

[19] Amis AA, Firer P, Mountney J, Senavongse W, Thomas NP. The anatomy and reconstruction of the medial patellofemoral ligament. Knee 2003;10:215–20.

[20] Grood ES, Suntay WJ. A Joint Coordinate System for the Clinical Description of Three-Dimensional Motions: Application to the Knee. J Biomech Eng 1983;105:136–44.

[21] Taylor R. Interpretation of the Correlation Coefficient: A Basic Review. J Diagnostic Med Sonogr 1990;6 :35–9.

[22] Fluit R, Andersen MS, Kolk S, Verdonschot N, Koopman HFJM. Prediction of ground reaction forces and moments during various activities of daily living. J Biomech 2014;47:2321–9.

[23] Baldwin MA, Clary CW, Fitzpatrick CK, Deacy JS, Maletsky LP, Rullkoetter PJ. Dynamic finite element knee simulation for evaluation of knee replacement mechanics. J Biomech 2012;45:474–83.

[24] Athwal KK, Hunt NC, Davies AJ, Deehan DJ, Amis A a. Clinical biomechanics of instability related to total knee arthroplasty. Clin Biomech 2014;29:119–28.

[25] Dennis D a, Komistek RD, Colwell CE, Ranawat CS, Scott RD, Thornhill TS, et al. In Vivo Anteroposterior Femorotibial Translation of Total Knee Arthroplasty: A

Multicenter Analysis. Clin Orthop Relat Res 1998;353:47–57.

[26] Cromie MJ, Siston RA, Giori NJ, Delp SL. Posterior cruciate ligament removal contributes to abnormal knee motion during posterior stabilized total knee arthroplasty. J Orthop Res 2008;26:1494–9.

[27] Park SE, DeFrate LE, Suggs JF, Gill TJ, Rubash HE, Li G. Erratum to "The change in length of the medial and lateral collateral ligaments during in vivo knee flexion". Knee 2006;13:77–82.

[28] Delport H, Labey L, Innocenti B, De Corte R, Vander Sloten J, Bellemans J. Restoration of constitutional alignment in TKA leads to more physiological strains in the collateral ligaments. Knee Surgery, Sport Traumatol Arthrosc 2015;23:2159–69.

[29] Victor J, Mueller JKP, Komistek RD, Sharma A, Nadaud MC, Bellemans J. In Vivo Kinematics after a Cruciate-substituting TKA. Clin Orthop Relat Res 2010;468:807–14.

[30] Baldwin MA, Laz PJ, Stowe JQ, Rullkoetter PJ. Efficient probabilistic representation of tibiofemoral soft tissue constraint. Comput Methods Biomech Biomed Engin 2009;12:651–9.

[31] H. Bloemker K. Computational Knee Ligament Modeling Using Experimentally Determined Zero-Load Lengths. Open Biomed Eng J 2012;6:33–41.

[32] Beillas P, Lee SW, Tashman S, Yang KH. Sensitivity of the tibio-femoral response to finite element modeling parameters. Comput Methods Biomech Biomed Engin 2007;10:209–21.

[33] Pandy MG, Sasaki K, Kim S. A Three-Dimensional Musculoskeletal Model of the Human Knee Joint. Part 1: Theoretical Construction. Comput Methods Biomech Biomed Engin 1997;1:87–108.

9. Tables

Table 1: Reference strain (ϵ_r) and stiffness (k) values adapted from Blankevoort and Huiskes [17]. The literature values were slightly adapted since our model has two MCL bundles and one LCL bundle while their model has three bundles for both MCL and LCL. The stiffness was redistributed according to the number of bundles, MCL reference strain could be copied and the LCL reference strain was copied such that the bundle was tensioned in full extension. Both MPFL and LEPL consisted of three bundles and the reported parameter values were assigned to each bundle.

	MCL	LCL	MPFL	LEPL
ϵ_r	0.04	0.08	0.08	0.06
k (N)	4125	6000	2000	1000

Table 2: Summary of the different configurations of the sensitivity study. For each configuration, only one model parameter was perturbed while all other model parameters were kept constant.

Component	Measure	Low value	Initial value	High value
LCL tibia	Ant-pos	-3.5 mm	reference	+3.5 mm
	Prox-dis	-3.5 mm	reference	+3.5 mm
LCL femur	Ant-pos	-3.5 mm	reference	+3.5 mm
	Prox-dis	-3.5 mm	reference	+3.5 mm
MCLprox tibia	Ant-pos	-3.5 mm	reference	+3.5 mm
	Prox-dis	-3.5 mm	reference	+3.5 mm
MCLprox femur	Ant-pos	-3.5 mm	reference	+3.5 mm
	Prox-dis	-3.5 mm	reference	+3.5 mm
MCLdist tibia	Ant-pos	-3.5 mm	reference	+3.5 mm
	Prox-dis	-3.5 mm	reference	+3.5 mm
MCLdist femur	Ant-pos	-3.5 mm	reference	+3.5 mm
	Prox-dis	-3.5 mm	reference	+3.5 mm
Patellar tendon tibia	Med-lat	-3.5 mm	reference	+3.5 mm
	Prox-dis	-3.5 mm	reference	+3.5 mm
Patellar tendon patella	Med-lat	-3.5 mm	reference	+3.5 mm
	Prox-dis	-3.5 mm	reference	+3.5 mm
LCL	k	5790 N	6000 N	6210 N
	ε_r	0.045%	0.08%	0.115%
MCLprox	k	3980N	4125 N	4270 N
	ε_r	0.005%	0.04%	0.075%
MCLdist	k	3980N	4125 N	4270 N
	ε_r	0.005%	0.04%	0.075%

Table 3: Comparison of measured and computed kinematics using RMSE and Pearson correlation coefficient ρ. Proximal-distal (PD), medial-lateral (ML), anterior-posterior (AP), varus-valgus (VV) and internal-external (IE) motions are shown.

	RMSE					ρ				
	PD (mm)	ML (mm)	AP (mm)	VV (°)	IE (°)	PD	ML	AP	VV	IE
Specimen 1										
Neutral	1.34	1.50	2.43	0.67	2.00	1.00	0.40	0.69	0.89	0.94
Varus	1.53	1.16	2.26	0.61	1.97	1.00	0.79	0.66	0.79	0.99
Valgus	0.89	2.19	2.58	0.41	2.91	1.00	-0.08	0.75	0.97	0.94
Specimen 2										
Neutral	0.47	0.89	2.95	0.80	2.65	1.00	0.00	0.91	0.93	0.92
Varus	0.44	0.65	2.18	1.26	3.23	1.00	0.88	0.94	0.99	0.93
Valgus	0.53	0.44	2.41	0.65	2.04	1.00	0.78	0.90	0.86	0.95
Specimen 3										
Neutral	1.38	0.93	3.26	0.45	1.94	0.99	0.43	0.97	1.00	0.97
Varus	1.52	1.82	3.13	0.75	1.58	0.99	-0.16	0.95	1.00	0.97
Average	1.01 ± 0.45	1.20 ± 0.56	2.65 ± 0.38	0.70 ± 0.25	2.29 ± 0.53	1.00 ± 0.00	0.38 ± 0.39	0.85 ± 0.12	0.93 ± 0.07	0.95 ± 0.02

Table 4: Comparison of experimental and computed ligament length changes using RMSE and Pearson correlation coefficient ρ. Kinematic based length changes (Kin) and extensometer length changes (Ext) are shown.

	RMSE				ρ			
	MCL Ext (%)	MCL Kin (%)	LCL Ext (%)	LCL Kin (%)	MCL Ext	MCL Kin	LCL Ext	LCL Kin
Specimen 1								
Neutral	1.88	0.87	3.45	3.26	0.98	0.99	0.25	0.99
Varus	4.64	1.11	1.99	3.44	0.97	0.99	0.28	0.97
Valgus	2.24	1.09	4.07	1.49	0.96	0.97	0.67	0.95
Specimen 2								
Neutral	2.08	0.44	4.97	1.74	0.99	1.00	0.95	0.97
Varus	2.03	0.76	4.05	2.25	0.94	0.99	0.99	0.98
Valgus	1.87	0.65	3.04	1.39	0.96	0.97	0.98	0.99
Specimen 3								
Neutral	2.83	1.27	5.92	2.73	0.93	0.99	0.87	0.98
Varus	3.95	1.10	4.73	3.82	0.92	0.99	0.92	0.98
Average	2.69 ±0.98	0.91 ±0.26	4.03 ±1.14	2.51 ±0.88	0.96 ±0.02	0.99 ±0.01	0.74 ±0.29	0.98 ±0.01

Figure legends

Figure 1: Illustration of the analytical surfaces that were fitted to the bone and implant geometries as wrapping surfaces. One cylinder was placed medially, allowing the MCLdist to wrap around the medial tibial condyle. Another cylinder was fitted to the femoral implant to prevent the quadriceps muscle from penetrating the implant in deep flexion. Two ellipsoids were introduced to wrap the MPFL and LEPL around the femoral condyles.

Figure 2: Illustration of the simulation of the mechanical rig inside AnyBody. The hip joint has 2 DOFs: vertical translation and flexion-extension. The ankle joint has 4 DOFs: all three rotations and medio-lateral translation. This configuration provides the tibio-femoral joint with all six DOFs. The patello-femoral joint was modelled with the assumption of a constant length for the patellar tendon and the other 5 DOF were solved using FDK.

Figure 3: Comparison of experimental and model tibio-femoral translations of the three specimens. Experimental (marker) and computed (line) proximal-distal (black/circles), medial-lateral (red/crosses) and anterior-posterior (blue/squares) translations are shown. The rows show the results for the different specimens, the columns show the results for the different configurations (varus insert, neutral insert and valgus insert).

Figure 4: Comparison of experimental and model tibio-femoral rotations of the three specimens. Experimental (marker) and computed (line) varus-valgus (black/circles) and internal-external (red/crosses) rotations are shown. The rows show the results for the different specimens, the columns show the results for the different configurations (varus insert, neutral insert and valgus insert).

Figure 5: 2D view of experimental (dotted lined) and model kinematics (full line) of the three specimens. The centres of the medial and lateral femoral condy

les are projected onto the tibial horizontal plane for different flexion angles (40°, 60°, 80° and 100°). The rows show the results for the different specimens, the columns show the results for the different configurations (varus insert, neutral insert and valgus insert). The top view of each specimen's left knee is depicted, with the anterior side pointing upwards.

Figure 6: Comparison of kinematic based experimental and model ligament length changes of the three specimens. Experimental (marker) and computed (line) MCLdist (black/circles) and LCL (red/crosses) strains are shown. The rows show the results for the different specimens, the columns show the results for the different configurations (varus insert, neutral insert and valgus insert).

Figure 7: The different output curves of the sensitivity analysis are shown as a shaded area on the figures. The first column shows translations, the second column rotations and the third and fourth column ligament length changes for the neutral configuration of each specimen (rows). The experimental measured data is shown in dotted line and the simulation with reference values in full line. For the translations, proximal-distal (red). medial-lateral (blue) and anterior-posterior (green) is shown. For the rotations, varus-valgus (red) and internal-external (blue) is depicted.

Figure 1

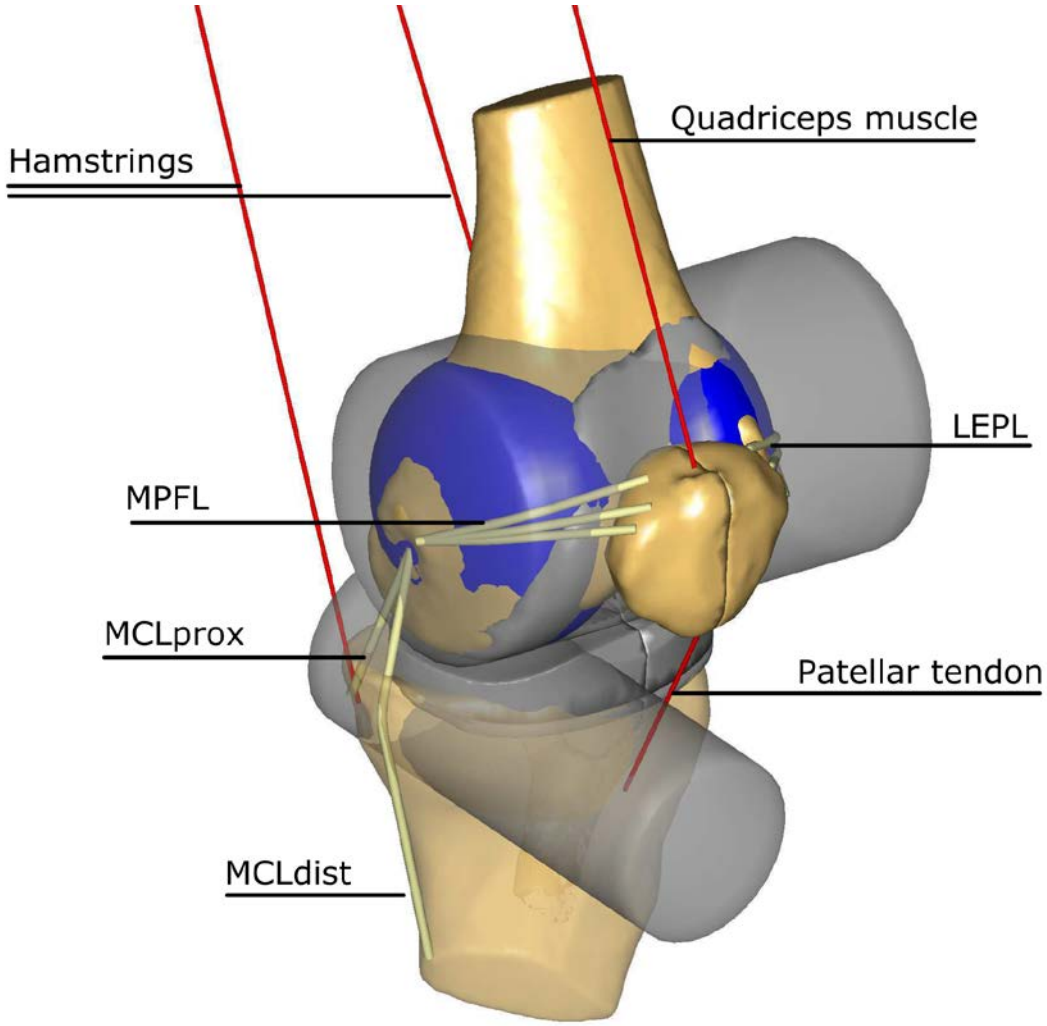

Figure 2

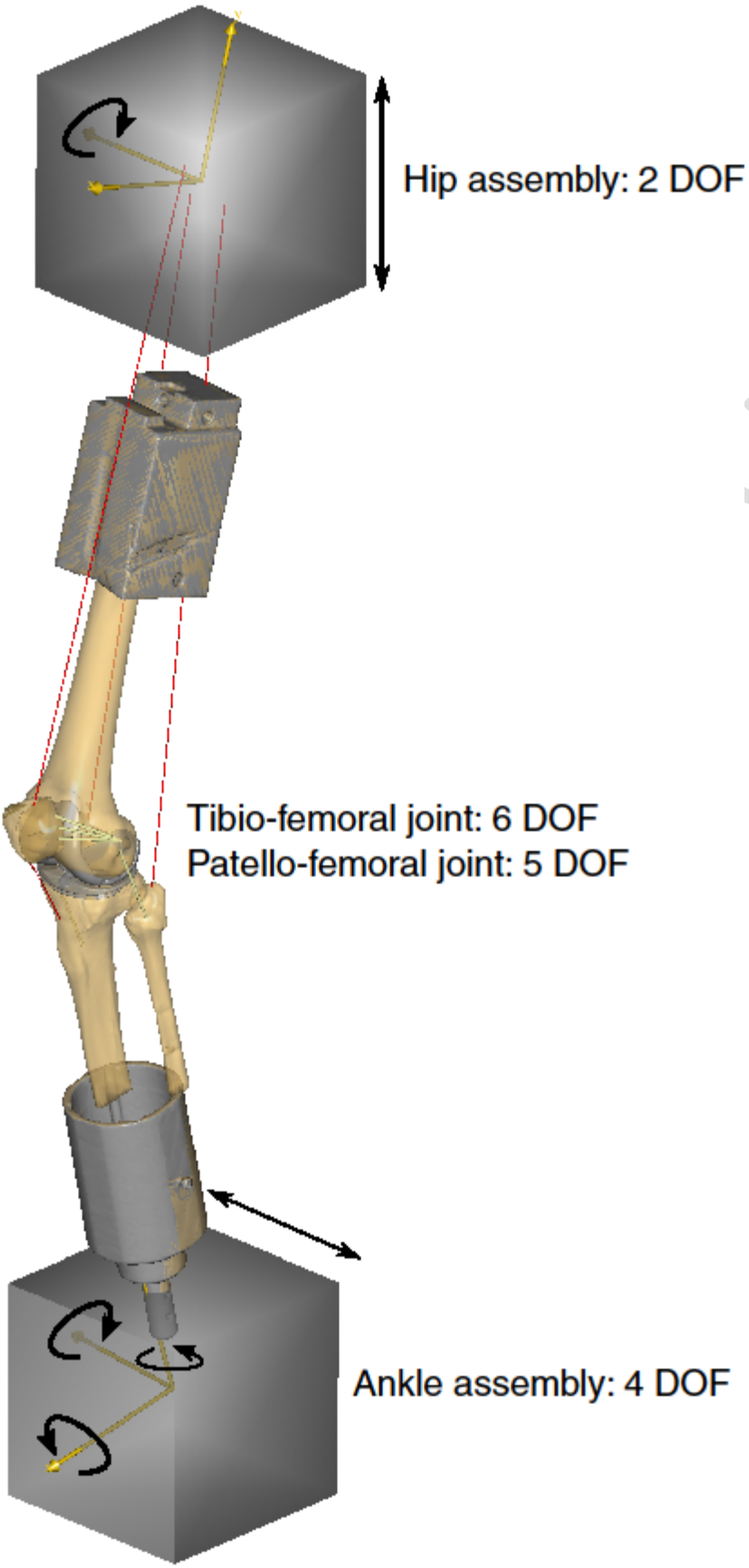

Figure 3

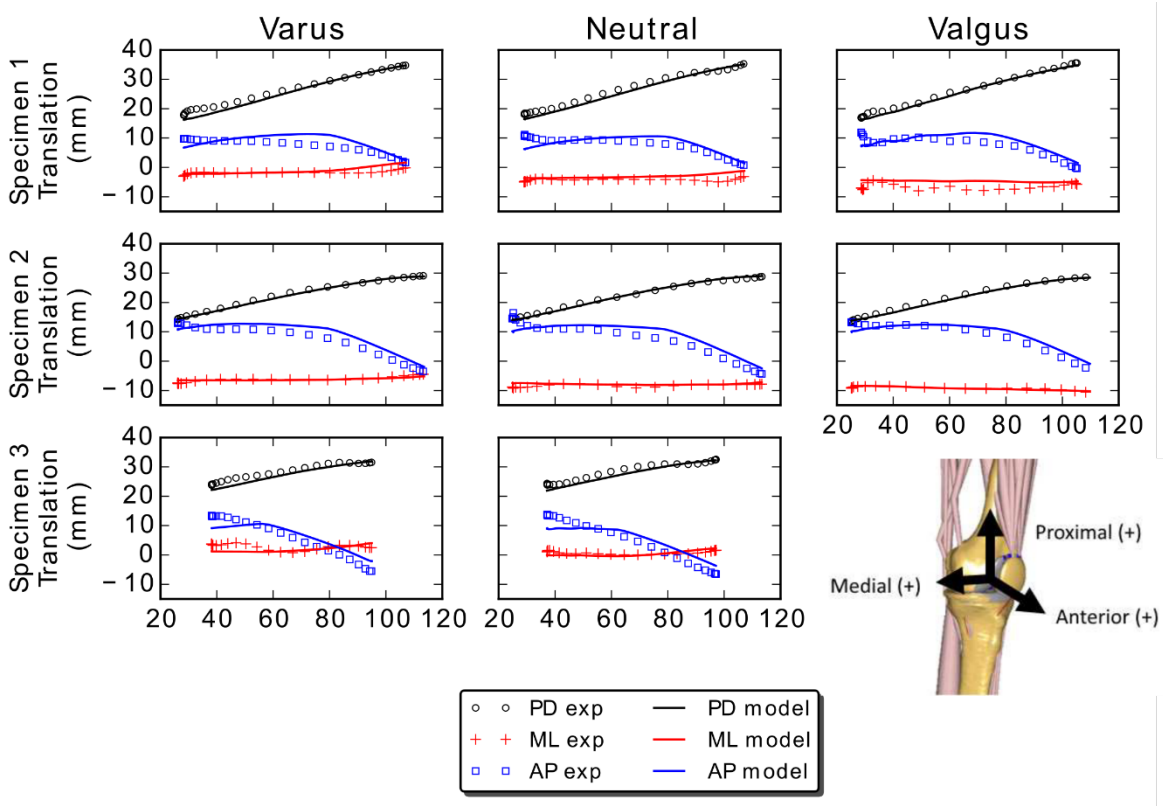

Figure 4

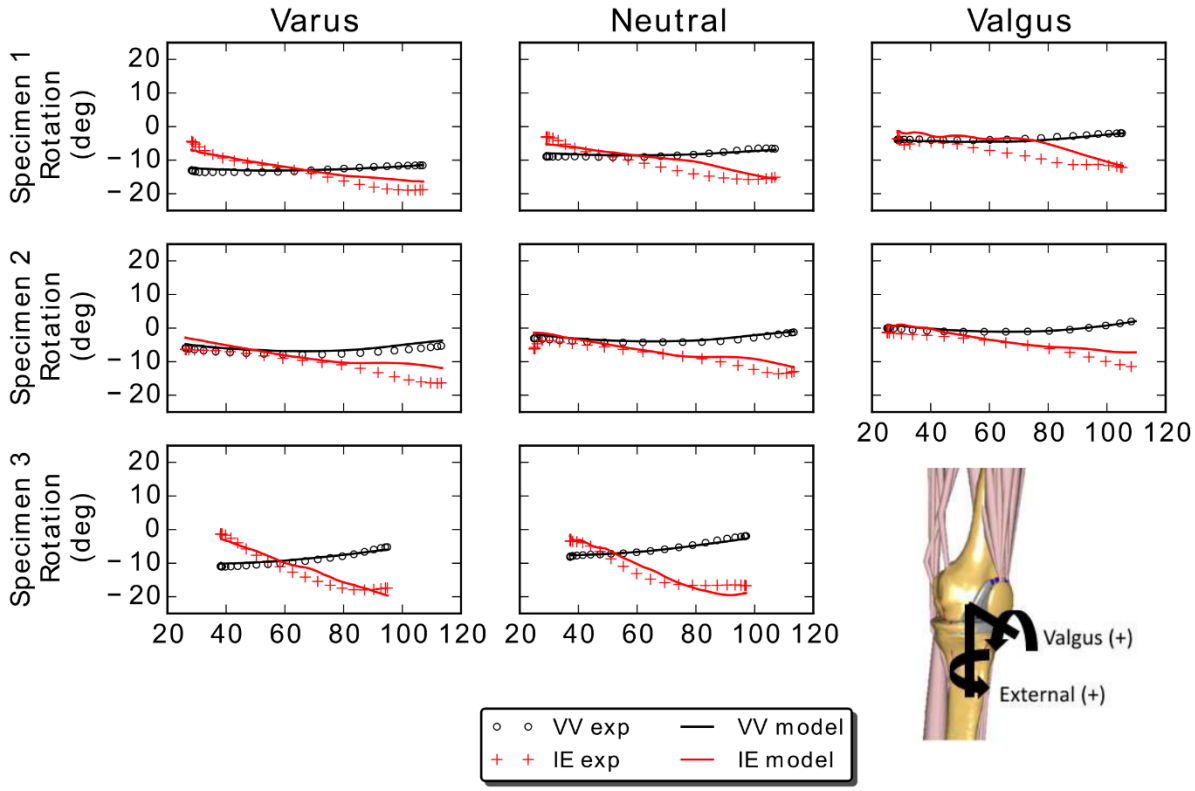

Figure 5

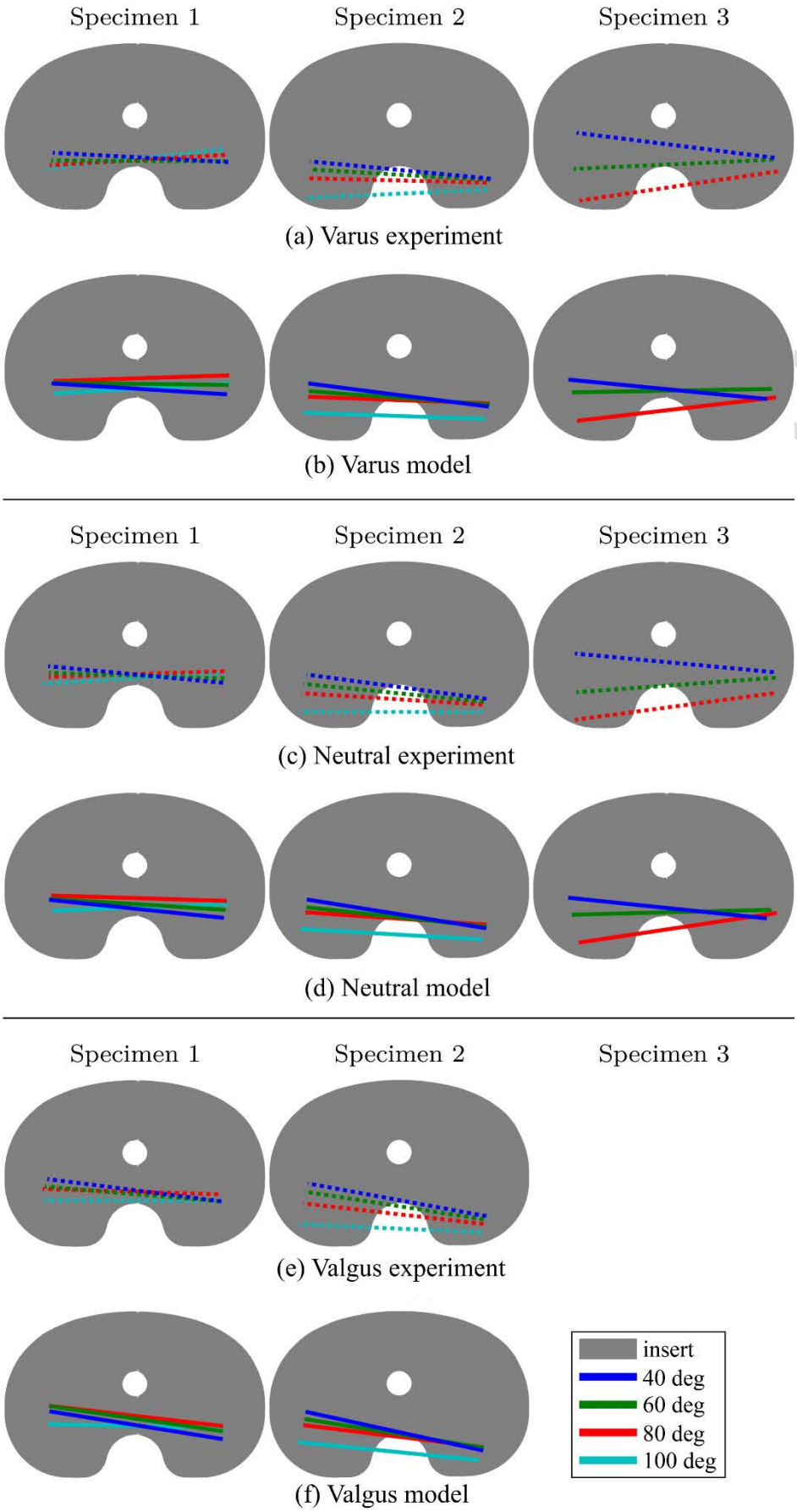
Specimen 1
Specimen 2
Specimen 3
(a) Varus experiment
(b) Varus model
Specimen 1
Specimen 2
Specimen 3
(c) Neutral experiment
(d) Neutral model
Specimen 1
Specimen 2
Specimen 3
(e) Valgus experiment
(f) Valgus model
insert
40 deg
60 deg
80 deg
100 deg

Figure 6

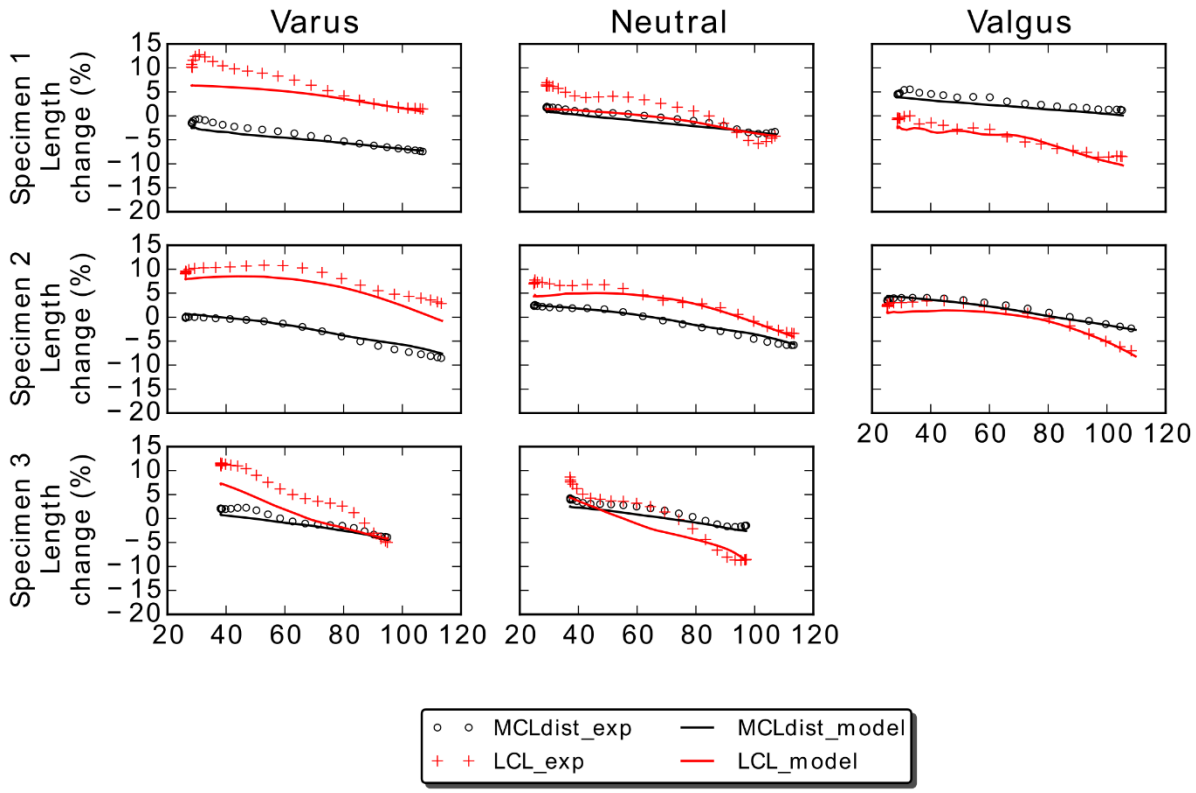

Figure 7

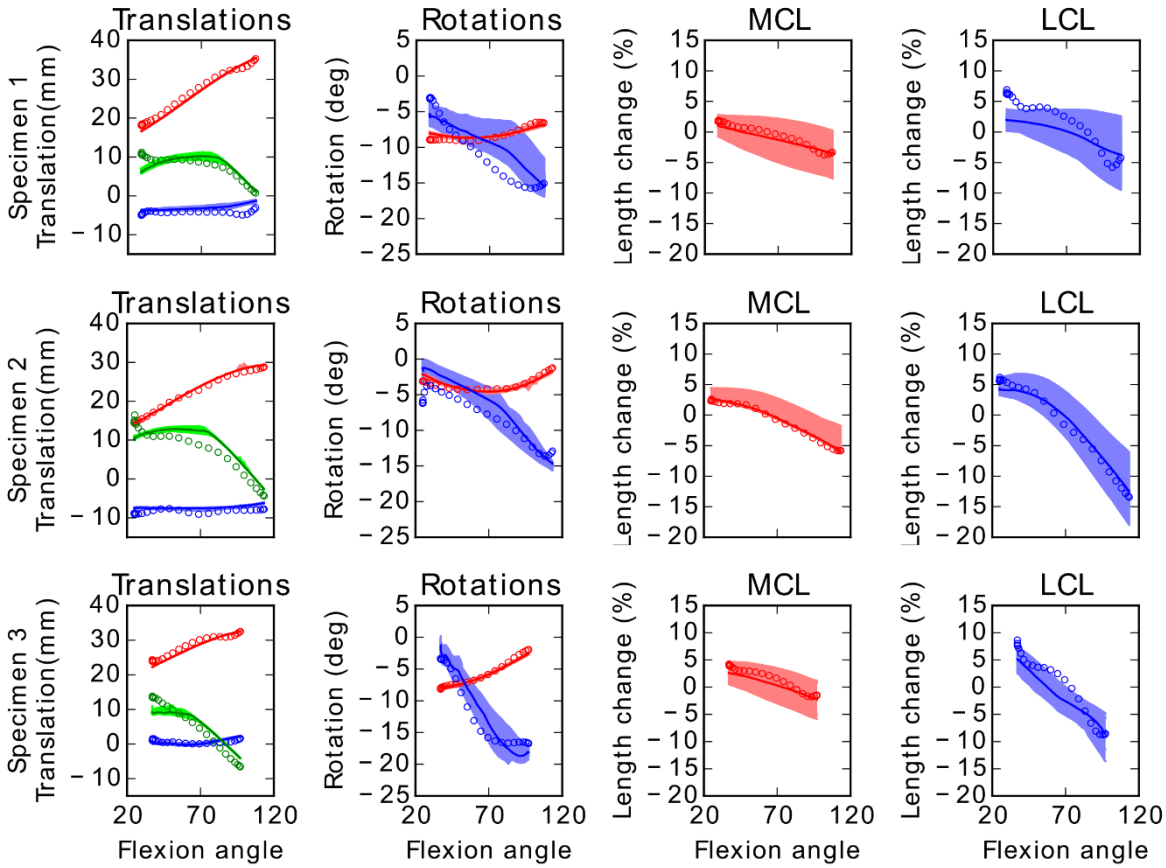
Translations
Rotations
MCL
LCL
Specimen 1
Specimen 2
Specimen 3
Translation(mm)
Rotation (deg)
Length change (%)
Flexion angle
20
70
120